THE JOURNAL OF PHYSICAL CHEMISTRY C

Article

pubs.acs.org/JPCC

Multinuclear Solid-State NMR Studies on the Formation Mechanism of Aluminophosphate Molecular Sieves in Ionic Liquids

Renshun Xu,[†] Weiping Zhang,*[,‡] Jun Xu,[§] Zhijian Tian,[†] Feng Deng,[§] Xiuwen Han,[†] and Xinhe Bao*[,†]

[†]State Key Laboratory of Catalysis, Dalian National Laboratory for Clean Energy, Dalian Institute of Chemical Physics, Chinese Academy of Sciences, Dalian 116023, China

[‡]State Key Laboratory of Fine Chemicals, Dalian University of Technology, 2 Linggong Road, Dalian 116024, China

[§]State Key Laboratory of Magnetic Resonance and Atomic and Molecular Physics, Wuhan Center for Magnetic Resonance, Wuhan Institute of Physics and Mathematics, Chinese Academy of Sciences, Wuhan 430071, China

Supporting Information

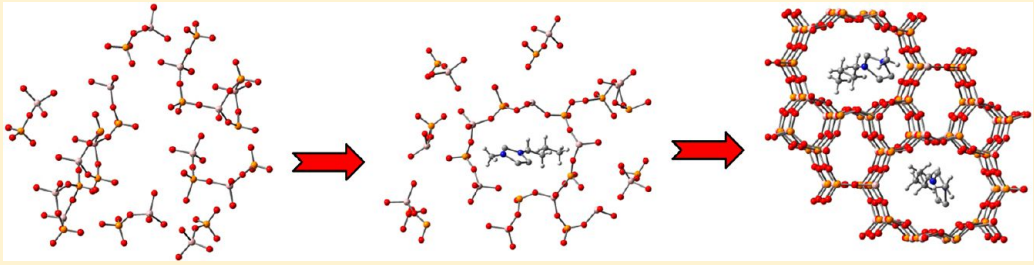

ABSTRACT: In the present work, multinuclear solid-state NMR techniques together with power X-ray diffraction (XRD) and scanning electron microscopy (SEM) were employed to monitor the crystallization process of aluminophosphate $AlPO_4$-11 molecular sieves in 1-ethyl-3-methylimidazolium bromide ([emim]Br) ionic liquids (ILs). The local environments of the selected solid samples were probed by one-dimensional ^{27}Al, ^{31}P, and ^{19}F MAS NMR experiments, and more information was obtained from two-dimensional $^{27}Al \rightarrow {}^{31}P$ heteronuclear correlation (HETCOR) and ^{27}Al triple-quantum MAS (3Q MAS) experiments. It is found that a large amount of amorphous aluminophosphates was formed with the $F-Al_{oct}-O-P_{par}$ and $Al_{tet}-O-P_{par}$ structures in the initial stage of aging. With increasing crystallization time, the partially condensed framework phosphorus species disappeared gradually and became fully condensed. Meanwhile, the octahedral Al was transformed into the pentahedral and tetrahedral Al species with the structures of $F-Al_{penta}-O-P_{ful}$ and $Al_{tet}-O-P_{ful}$ in the $AlPO_4$-11 frameworks. During the crystallization process, [emim] cations acting as the structure-directing agents were occluded into the channels, and F^- anions were connected with pentahedral Al in the final AlPO4−11 phase. All of these findings can allow proposing a possible formation mechanism for the synthesis of $AlPO_4$-11 in ionic liquids.

INTRODUCTION

Because of a wide range of practical applications, the synthesis of molecular sieves with diverse compositions, structures, and properties is important from both fundamental and technological points of view.[1] Although new molecular sieves are being regularly discovered, the rational "priori design" of molecular sieves now is still a challenge because of the lack of full understanding of the synthesis mechanism. A more comprehensive knowledge of the fundamental processes occurring during the crystallizations would be of great value. During the past decade, many advanced methods including X-ray adsorption technique,[2] UV Raman[3] and NMR,[4] etc., have been applied to study the molecular sieves crystallizations. Among them, NMR is a powerful tool that can probe the local or atomic environments of both solid and liquid phases. The crystallization process of molecular sieves investigated by solid-state NMR has provided valuable insights into the nucleation and crystal growth.[5] In recent years, a novel preparation method for molecular sieves, termed as ionothermal synthesis, was reported by Morris et al. using ionic liquids (ILs) or eutectic mixture as both solvent and template.[6] Unlike hydrothermal or solvothermal synthesis, the reaction takes place in an ionic environment in ionothermal synthesis. Also, it can be performed at ambient pressure due to the vanishingly low vapor pressure of almost all ILs. To date, a series of aluminophosphate aluminosilicate molecular sieves, metal−organic frameworks, and zeolite films, etc., have been synthesized using ILs as both solvents and structure-directing agents (SDAs).[7] Moreover, the ionothermal synthesis exhibits some distinct characteristics. Taking the synthesis of $AlPO_4$-11 as an example, as compared to its synthesis in hydrothermal synthesis,[5b] the crystallization time is very short in ionothermal synthesis. However, the formation mechanism of aluminophosphate molecular sieves in ionic liquids is still not well

Received: January 14, 2013
Revised: February 22, 2013
Published: February 25, 2013

established. In this work, the synthesis process of $AlPO_4$-11 molecular sieves in 1-ethyl-3-methylimidazolium bromide [emim]Br ionic liquids was investigated by one- and two-dimensional multinuclear MAS NMR, XRD, and SEM. The phase transition from amorphous state to the stable $AlPO_4$-11 in the final solids was described through the detailed characterization information on the atomic level. A possible evolution mechanism of $AlPO_4$-11 in ionic liquids was also proposed. Our findings may open a new recognition in the ionothermal synthesis of molecular sieves.

EXPERIMENTAL SECTION

Sample Preparation. $AlPO_4$-11 was ionothermally synthesized similarly to our previous procedures in which the gel had a composition of $40[emim]Br:1.0Al_2O_3:3.0P_2O_5:0.5HF$.[5e−g,7e−g] $Al(OPr_i)_3$ (triisopropylate aluminum) and H_3PO_4 (85 wt %) were used as the sources of aluminum and phosphorus, respectively. In general, $Al(OPr_i)_3$, H_3PO_4, and HF acid were added to the [emim]Br ILs under stirring, and the initial mixtures were aged at 363 K for about 1 h. The gels then were heated to 443 K for crystallization. The reaction was quenched by an ice bath at different stages. The solid products were filtered and washed with distilled water and ethanol, and dried thoroughly in air at room temperature.

Characterizations. All samples were characterized by powder X-ray diffraction on a Rigaku D/Max-2500 diffractometer using Cu Kα radiation. SEM observation was carried out using a field-emission scanning microscope model FEI Quanta 200F working under low accelerated voltage.

Solid-state NMR measurements were performed on the Varian Infinityplus-400 spectrometer operating at a magnetic field strength of 9.4 T. ^{27}Al MAS NMR spectra were recorded at 104.2 MHz with a spinning rate of 10 kHz, 200 scans, and 2 s recycle delay. The chemical shifts were referenced to 1% $Al(NO_3)_3$ aqueous solution. ^{31}P MAS NMR experiments with high power proton decoupling and the $^1H\rightarrow^{31}P$ CP/MAS experiment were conducted at 161.8 MHz with a spinning rate of 10 kHz and 4 s recycle delay. The chemical shifts were referenced to 85% H_3PO_4. ^{19}F MAS spectra were recorded at 376.4 MHz with spinning rate of 14 kHz and a recycle delay of 20 s. The chemical shifts were referenced to trifluoroacetic acid. $^{19}F\rightarrow^{27}Al$ CP/MAS experiments were optimized on the completely crystallized $AlPO_4$-11 sample; the spinning rate is 6 kHz. Two-dimensional ^{27}Al triple-quantum (3Q) MAS NMR experiments were performed using a three-pulse sequence incorporating a z-filter at a spinning speed of 25 kHz with the 2.5 mm probe.[8] In the $^{31}P\{^{27}Al\}$ TRAPDOR experiment, a spin−echo pulse sequence was applied to the ^{31}P spins while ^{27}Al nuclei were irradiated in an alternating fashion. The rf field strength for ^{27}Al irradiation was 50 kHz, the pulse delay was 180 s, and the irradiation time equals multiples of the rotor period (0.25 ms) with spinning rate of 4 kHz. Two-dimensional $^{27}Al\rightarrow^{31}P$ heteronuclear correlation (HETCOR) spectra were acquired using the approach described by Fyfe et al.[9] The TPPI method was used in the 2D data acquisition and processing. $^1H\rightarrow^{13}C$ CP/MAS NMR spectra were recorded at 100.5 MHz with spinning rate of 4 kHz, 6000 scans, 2.5 ms contact time, and 2 s recycle delay. The chemical shifts were referenced to the adamantane with the upfield methine peak at 29.5 ppm.

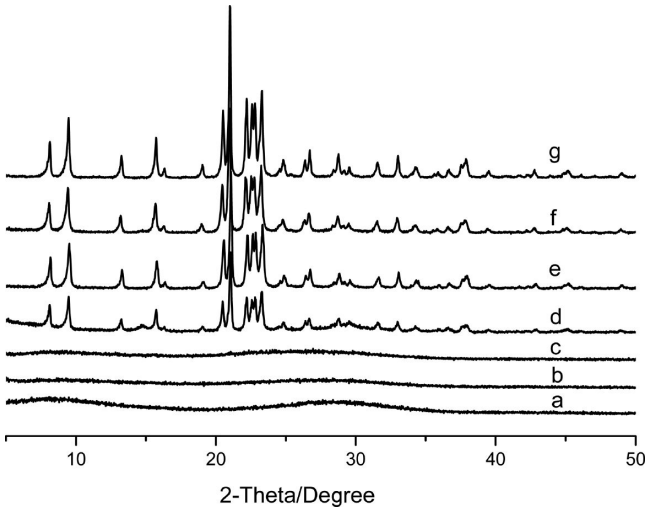

Figure 1. XRD patterns of the solid samples aged at 363 K (a), and crystallized at 443 K for different time, 0 min (b), 15 min (c), 20 min (d), 35 min (e), 70 min (f), and 120 min (g).

RESULTS AND DISCUSSION

Powder XRD and SEM. The powder XRD patterns of the solid samples synthesized in ionic liquids with different crystallization time are presented in Figure 1. The initial solid samples aged at 363 K contain only a broad signal, indicating the amorphous materials in the sample. Increasing the temperature to 443 K, XRD patterns are still identical and contain only a broad signal in Figure 1b,c. When prolonging the crystallization time to 20 min, some sharp peaks appear in Figure 1d, which means a part of crystallines with the long-range ordering were formed. However, the intensities of the peaks assigned to $AlPO_4$-11 are weak, which indicates that there are a large amount of amorphous materials existing in the samples. Further increasing the crystallization time, the intensity of the diffraction peaks is remarkably increased. Heating the gel for 70 min or longer time leads to completely crystallized $AlPO_4$-11. It can be concluded from the XRD patterns that the phase transition from amorphous state to the stable $AlPO_4$-11 only needs 1−2 h, and the crystallization rate of ionothermal synthesis is very fast.

The morphologies of the selected solid samples during the synthesis process were investigated by SEM. As shown in Figure 2a, the initial solid samples aged at 363 K are small aggregates; it could be amorphous aluminophosphate formed by the partial condensation of aluminum and phosphorus species. Increasing the temperature to 443 K for crystallization, the morphologies of the solid samples are similar to the initial gel particles in Figure 2b. Increasing the crystallization time to 20 min, some stick-like $AlPO_4$-11 crystal could be observed besides the amorphous particles in Figure 2c, which agrees well with the formation of $AlPO_4$-11 phase during this stage as detected by XRD. After 120 min of ionothermal treatment, rod-shaped crystals with length of about 300 nm are formed as shown in Figure 3d. This means all amorphous aluminophosphate was transformed into $AlPO_4$-11 at the final stage.

^{27}Al and ^{31}P MAS NMR. The local structures of aluminum in the selected samples were detected by ^{27}Al MAS NMR as shown in Figure 3. For the initial solid samples aged at 363 K, a strong peak at −12 ppm and a very weak peak at ca. 46 ppm can be observed. The former peak should come from the octahedral Al, and the latter peak could be associated with the

dx.doi.org/10.1021/jp400422z | J. Phys. Chem. C 2013, 117, 5848−5854

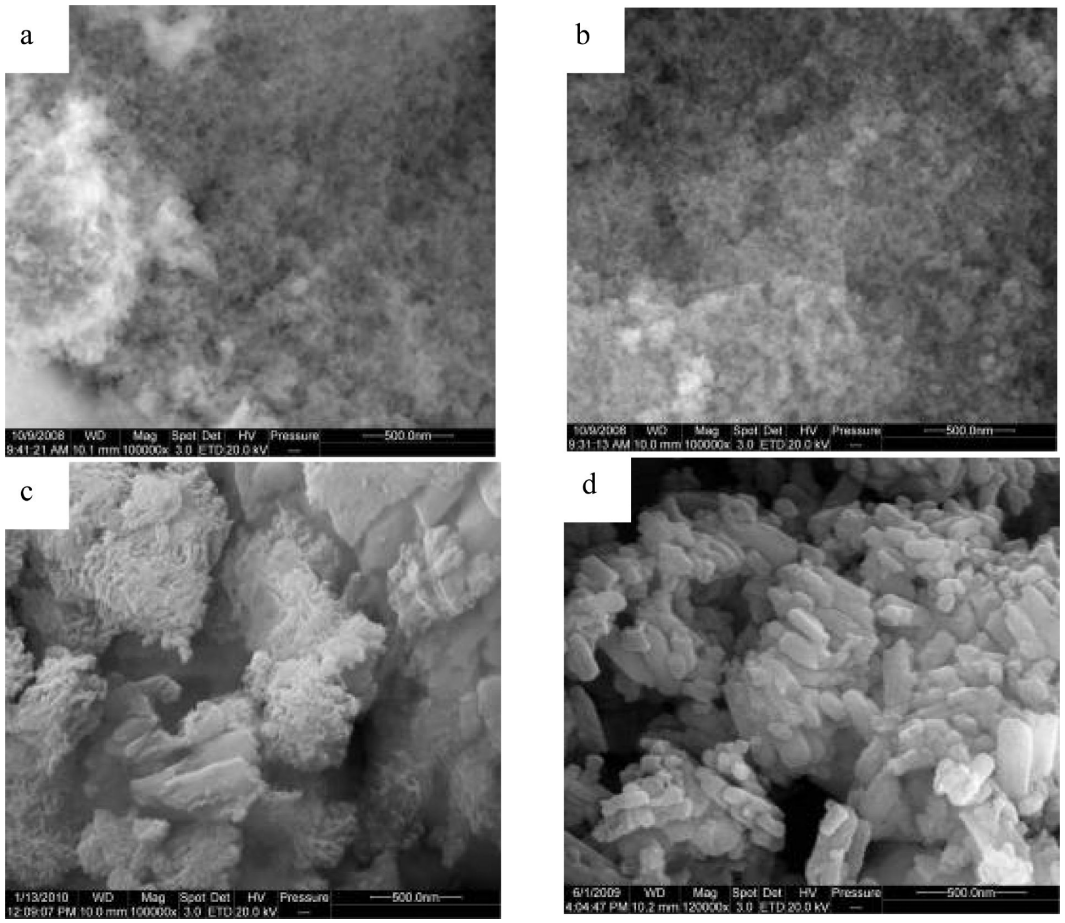

Figure 2. SEM images of the solid samples aged at 363 K (a), and crystallized at 443 K for different time, 0 min (b), 20 min (c), and 120 min (d).

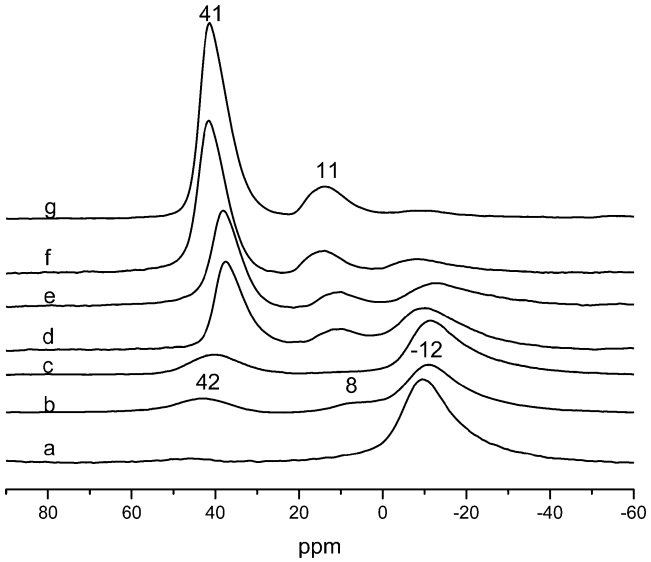

Figure 3. ^{27}Al MAS NMR spectra of the solid samples aged at 363 K (a), and crystallized at 443 K for different time, 0 min (b), 15 min (c), 20 min (d), 35 min (e), 70 min (f), and 120 min (g).

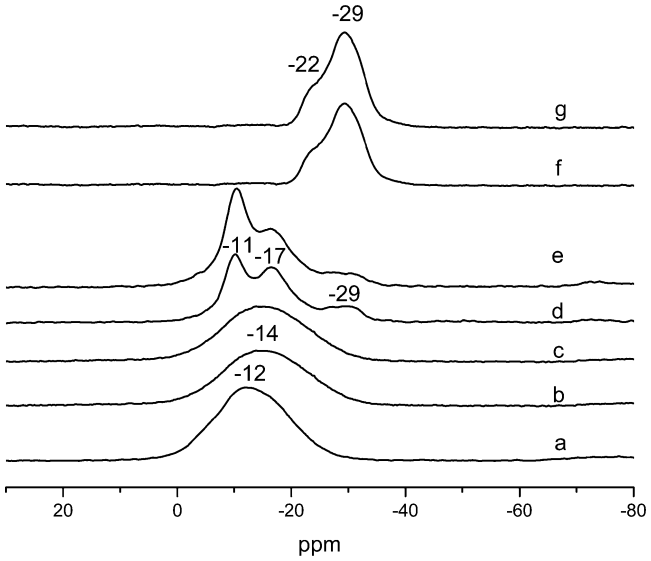

Figure 4. ^{31}P MAS NMR spectra of the solid samples aged at 363 K (a), and crystallized at 443 K for different time, 0 min (b), 15 min (c), 20 min (d), 35 min (e), 70 min (f), and 120 min (g).

tetrahedral Al in the amorphous aluminophosphate.[5c,10] Upon the crystallization at 443 K, the ^{27}Al MAS spectrum contains a weak peak at ca. 42 ppm and a strong peak at −12 ppm with a shoulder between them at about 8 ppm in Figure 3b. The shoulder signal at 8 ppm should be ascribed to the pentacoordinated Al instead of the octahedral Al resonance with asymmetric line shape, which is further confirmed by two-dimensional 3Q ^{27}Al MAS NMR spectrum (see Figure S1a in the Supporting Information). For the sample crystallized for 15 min, the ^{27}Al MAS NMR spectrum shows the similar feature to

dx.doi.org/10.1021/jp400422z | J. Phys. Chem. C 2013, 117, 5848−5854

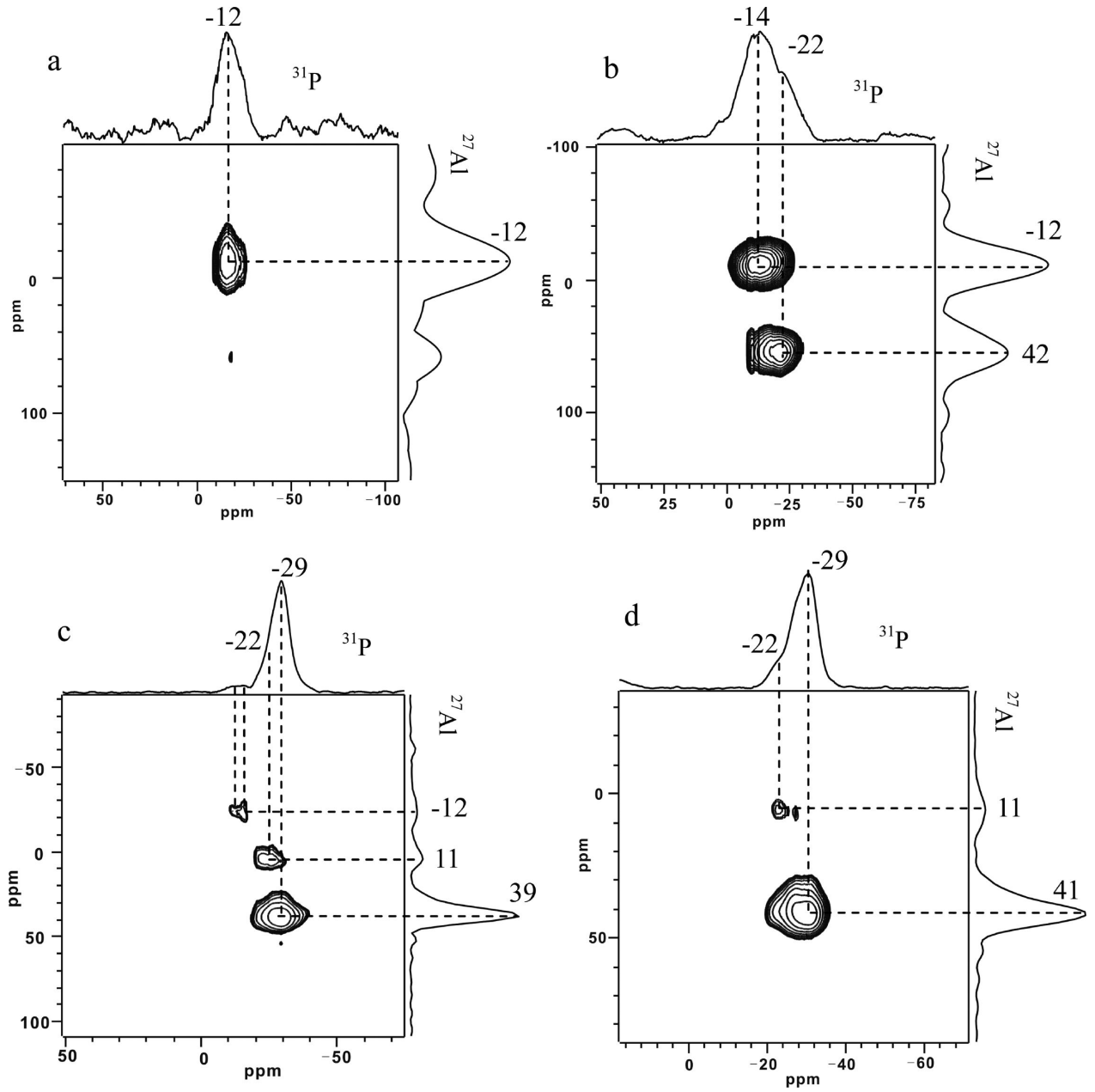

Figure 5. ^{27}Al→^{31}P HETCOR spectra of the solid sample aged at 363 K (a), and crystallized at 443 K for different time, 0 min (b), 20 min (c), and 120 min (d).

the 0 min sample at 443 K except for the disappearance of the peak at 8 ppm. With increasing crystallization time, the intensity of tetrahedral Al increases at the expense of octahedral Al, and a new weak signal at 11 ppm appears. The ^{27}Al signal at about 11 ppm should be also assigned to the pentacoordinated Al as indicated by the 3Q ^{27}Al MAS NMR spectrum (see Figure S1b in the Supporting Information).[11] This signal may be associated with the F−Al complexes as suggested by Xu et al.[5d] and Gougeon et al.[12] For the sample crystallized for 120 min, the peak of tetrahedral Al is dominant with a shoulder peak of pentacoordinated Al, which corresponds to the completely crystallized $AlPO_4$-11.

The local structures of phosphorus in the samples during the crystallization process were also probed by the ^{31}P MAS NMR as shown in Figure 4. The ^{31}P MAS spectrum of the solid samples aged at 363 K shows a broad signal at ca. −12 ppm. For the solid samples crystallized at 443 K for 0 and 15 min, the position of the ^{31}P signal shifts a little to −14 ppm. Both signals can be assigned to the partially condensed phosphate species in amorphous aluminophosphates.[13] For the sample crystallized for 20 min, the ^{31}P MAS spectrum shows two well-resolved peaks at −11 and −17 ppm, and a relatively weak signal at ca. −29 ppm. The assignments of these three peaks are verified by the ^{1}H→^{31}P cross-polarization (CP) MAS experiments (see Figure S2 in the Supporting Information). With shorter contact time, only the signals at −11 and −17 ppm can be observed in ^{1}H→^{31}P CP/MAS NMR spectra. With increasing contact time, the weak signal at −29 ppm becomes stronger. For the $I = 1/2$ nucleus system, the CP efficiency is intimately associated with the heteronuclear dipolar−dipolar interaction that is inversely proportional to the internuclear distance.[14] The low CP efficiency of the signal at −29 ppm from the $[emim]^+$ protons

dx.doi.org/10.1021/jp400422z | J. Phys. Chem. C 2013, 117, 5848−5854

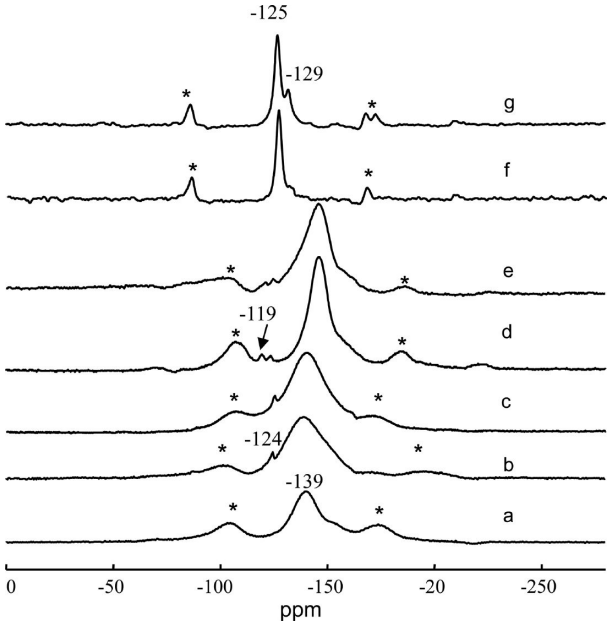

Figure 6. ^{19}F MAS NMR spectra of the solid sample aged at 363 K (a), and crystallized at 443 K for different time, 0 min (b), 15 min (c), 20 min (d), 35 min (e), 70 min (f), and 120 min (g). "*" indicates the spinning sidebands.

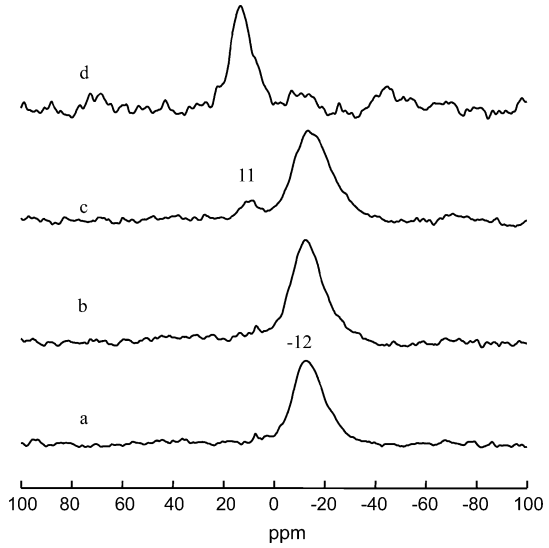

Figure 7. $^{19}F \rightarrow ^{27}Al$ CP/MAS NMR spectra of the solid sample aged at 363 K (a), and crystallized at 443 K for different time, 0 min (b), 20 min (c), and 120 min (d). Contact time is 0.5 ms.

or the H_2O protons can be ascribed to the fully condensed coordination sphere around the P sites in the $AlPO_4$-11 crystalline framework.[13] By contrast, the high CP efficiency of the signals at −11 and −17 ppm from their adjacent OH groups can be ascribed to the partially condensed P-$(OAl)_2(OH)_2$ and $P(OAl)_3OH$, respectively, in the $AlPO_4$-11 crystalline framework. Further lengthening the crystallization time leads to the growth of the signals at −22 and −29 ppm and a remarkable decrease of the signals at −11 and −17 ppm. For the sample crystallized for 70 and 120 min, the ^{31}P MAS NMR spectrum corresponds to the completely condensed P sites in the $AlPO_4$-11 crystallines.

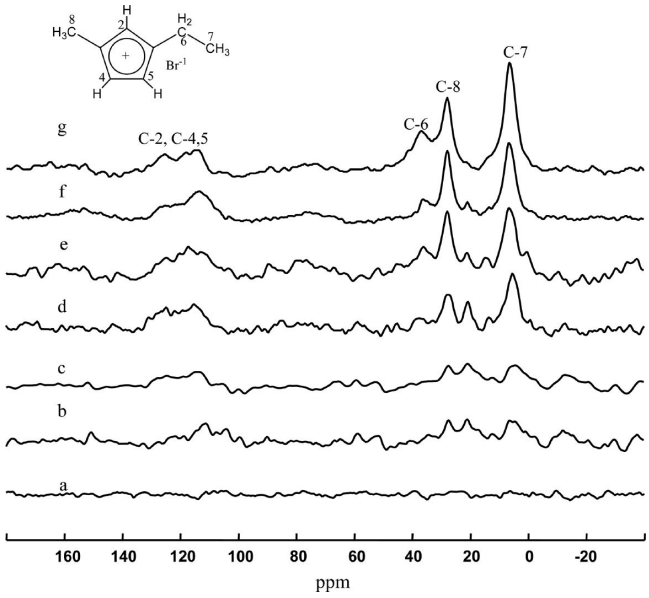

Figure 8. $^{1}H \rightarrow ^{13}C$ CP/MAS NMR spectra of the solid sample aged at 363 K (a), and crystallized at 443 K for different time, 0 min (b), 15 min (c), 20 min (d), 35 min (e), 70 min (f), and 120 min (g).

Two-Dimensional $^{27}Al \rightarrow ^{31}P$ HETCOR NMR. The assignments of ^{27}Al and ^{31}P resonances of selected solid samples were further confirmed by $^{27}Al \rightarrow ^{31}P$ HETCOR NMR technique, which provides the connectivity information of ^{27}Al and ^{31}P via a dipolar interaction (Figure 5). For the initial sample at 363 K, the resonance at −12 ppm in the ^{31}P projection correlates more strongly with the octahedral Al at −12 ppm in the ^{27}Al projection. For the sample crystallized at 443 K for 0 min, two ^{31}P signals at −14 and −22 ppm appear in the ^{31}P projection, showing distinctly different patterns as compared to the corresponding ^{31}P MAS spectrum. The ^{31}P signal at −14 ppm correlates to the peak at −12 ppm of the ^{27}Al projection, while the ^{31}P signal at −22 ppm correlates to the ^{27}Al signal at 42 ppm. The ^{31}P signal at −22 ppm can be assigned to the fully condensed P bound to four Al atoms in its coordination sphere, while the signal at −14 ppm can be ascribed to the partially condensed P with less than four Al atoms in its coordination sphere.[5c,10] However, the shoulder signal at 8 ppm in the ^{27}Al MAS spectrum is invisible in the HETCOR spectrum, indicating that the Al atom does not connect with P atom and should be ascribed to unreacted aluminum resource. As for the sample crystallized for 20 min, the ^{31}P signal at −29 ppm correlates to the ^{27}Al signal at 39 ppm, the ^{31}P signal at −22 ppm correlates to the ^{27}Al signal at 11 ppm, while the ^{31}P signals at −12 and −17 ppm are only correlated to the octahedral Al sites at −12 ppm. It should be noted that the ^{31}P signal intensity at −29 ppm increases remarkably, while those at −12 and −17 ppm decrease as compared to the corresponding ^{31}P MAS spectrum. This result further demonstrates that the ^{31}P signal at −29 ppm is due to the $P(OAl)_4$ in crystalline framework. As for the well-crystallized $AlPO_4$-11 for 120 min, the ^{31}P signal at −22 ppm is correlated more strongly to the pentacoordinated Al at 11 ppm, while that at −29 ppm should be associated with the tetrahedral Al at 41 ppm.

^{19}F MAS and $^{19}F \rightarrow ^{27}Al$ CP/MAS NMR. Fluoride plays an important role in the synthesis of molecular sieves.[5d,15] The local structures of fluoride in the selected samples during the crystallization process were investigated by the ^{19}F MAS NMR

dx.doi.org/10.1021/jp400422z | J. Phys. Chem. C 2013, 117, 5848−5854

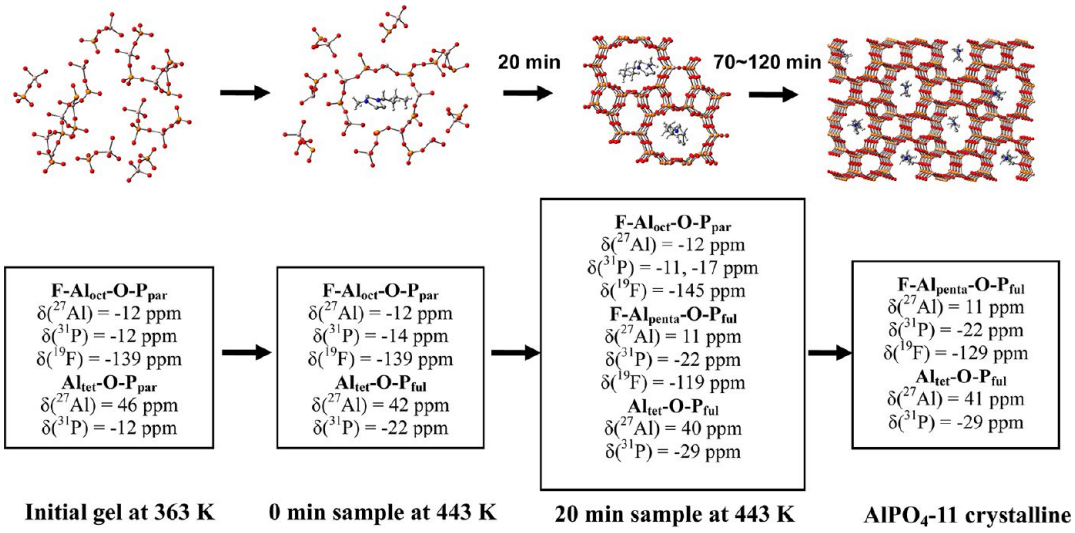

Figure 9. Evaluation of the ionothermal synthesis of $AlPO_4$-11 at different stages.

as shown in Figure 6. For the sample at 363 K, a broad signal at −139 ppm probably due to fluorine species in an amorphous phase can be observed. In Figure 6b,c, a new sharp signal at −124 ppm is detected in addition to the signal at −139 ppm. The ^{19}F signal at −124 ppm may be ascribed to either fluorine ions connecting with the pentacoordinated Al in AlPOs crystal or balancing the charge of template.[5d,g,12] Further prolonging the crystallization time to 20 or 35 min, the broad ^{19}F signal of amorphous phase shifts to −145 ppm, and two sharp ^{19}F peaks at −119 and −124 ppm can be detected. For the samples crystallized for 70 and 120 min, the sharp ^{19}F signals shift to the upfield, and the dominating fluorine resonance is at −125 ppm with a minor signal at −129 ppm.

To discriminate the connectivity of the F−Al complex, the selected samples are measured with ^{19}F→^{27}Al CP/MAS spectra as shown in Figure 7. For the initial sample at 363 K, ^{27}Al signal at −12 ppm corresponding to octahedral Al can be observed, so it is clear that the ^{19}F signal at −139 ppm can be ascribed to the octahedral F−Al complex. As for the 0 min sample at 443 K, the ^{19}F→^{27}Al CP spectrum still only shows a peak at −12 ppm. Therefore, the ^{19}F signal at −124 ppm should be due to fluorine ions balancing the charge of [emim]$^+$ cation, and could not be associated with the pentacoordinated Al. As for the sample crystallized for 20 min, a new ^{27}Al peak at 11 ppm, which is due to pentacoordinated Al, can be detected. From combination of the ^{19}F MAS spectrum, it can be concluded that the fluoride species at about −119 ppm are connected to the pentacoordinated Al in the solid sample. For the crystalline $AlPO_4$-11, the signal at 11 ppm arising from the framework pentacoordinated F−Al complex becomes the dominant peak. So, during the ionothermal synthesis of aluminophosphate molecular sieves, F^- anions not only play the role of balancing the [emim]$^+$ but also are involved in the formation of $AlPO_4$-11 framework.

^{1}H→^{13}C CP/MAS NMR. The state of organic moieties was analyzed by the ^{1}H→^{13}C CP/MAS NMR as shown in Figure 8. For the initial solid samples aged at 363 K, there are no signals of ionic liquids. For the solid samples crystallized at 443 K for 0 and 15 min, weak signals that are in accorded with the ^{13}C NMR signal of [emim]$^+$ cations can be observed. In our work, the isolated gels were washed thoroughly with deionized water before drying to avoid the remaining ILs. The weak signal suggests that a small amount of [emim]$^+$ cations interacts with the solid samples. With prolonging the crystallization time, the relative intensities of [emim]$^+$ cations are gradually increased indicating that more and more [emim]$^+$ cations were occluded in the channel of $AlPO_4$-11. Morris et al. have proposed that the ILs can act as structure-directing agents or pore filling agents in the ionothermal synthesis;[6] however, they only provided the evidence that ILs cations were occluded in the final crystalline product. In our work, the ^{1}H→^{13}C CP/MAS NMR results show that the [emim]$^+$ cations were intercalated into the inorganic frameworks as the structure-directing agents at the beginning of crystallization process, even though the formation of the AlPO framework has not been detected by XRD.

Formation Mechanism of $AlPO_4$-11 in ILs. On the basis of the above experimental results, the ionothermal synthesis of $AlPO_4$-11 can be clearly pictured as shown in Figure 9. After the synthesis reactants were mixed together at 363 K, the Al−O−P units are formed, resulting in a large amount of amorphous AlPO gel, and all the coordinated P atoms are partially condensed. The initial sample with the amorphous nature can be identified by two main components, which are composed of aluminophosphates species characterized by F−Al$_{oct}$−O−P$_{par}$ and Al$_{tet}$−O−P$_{par}$ (par donates partially condensed). Increasing temperature to 443 K for crystallization, the composition in AlPO gel is almost unchanged, but a small amount of [emim]$^+$ cations is occluded in the amorphous solids with F^- anions as the charge balance. Further lengthening the crystallization time, the morphology of gel particles undertakes stepwise change from amorphous into crystalline features, the Al sites in the form of Al$_{tet}$−O−P$_{par}$ gradually transform into Al$_{tet}$−O−P$_{ful}$, and the fully condensed P sites increase at the expense of the partially condensed P sites. Two microdomains can be clearly identified in the 20 min sample at 443 K: the periodic crystalline structure characterized by Al$_{tet}$−O−P$_{ful}$ and F−Al$_{penta}$−O−P$_{ful}$ units appears to be domain I, and the amorphous fluoroaluminophosphate characterized by F−Al$_{octa}$−O−P$_{par}$ is domain II. In the final stage, the amorphous components are nearly consumed and transformed into purely crystalline $AlPO_4$-11 characterized by F−Al$_{penta}$−O−P$_{ful}$ and Al$_{tet}$−O−P$_{ful}$ units with occlusion of [emim]$^+$ cations as the structure-directing agents.

dx.doi.org/10.1021/jp400422z | J. Phys. Chem. C 2013, 117, 5848−5854

As for the synthesis mechanism of molecular sieves, some researchers believe that the synthesis of zeolites involves the formation of nanoblocks, which then further combine to generate the extended framework of the crystal,[16] while some researchers believe that the crystallization is most probably from an amorphous gel.[17] In our study, the solid samples contain amorphous phase before the formation of purely crystalline $AlPO_4$-11, which support the $AlPO_4$ crystallization mechanism of transformations from the amorphous aluminophosphate phases.

CONCLUSIONS

XRD, SEM, one-, and two-dimensional multinuclear MAS NMR characterizations demonstrate that during the ionothermal synthesis of $AlPO_4$-11 a large amount of amorphous aluminophosphates is formed with the local structures of the $F-Al_{oct}-O-P_{par}$ and $Al_{tet}-O-P_{par}$ units in the initial stage of aging. After crystallization, the morphology of gel particles undertakes a stepwise change from amorphous into crystalline features. Meanwhile, the fully condensed P sites increase through the hydroxyl reaction with the octahedral Al, and the Al sites are gradually transformed into $F-Al_{penta}-O-P_{ful}$ and $Al_{tet}-O-P_{ful}$ units of the $AlPO_4$-11 frameworks. Ionic liquids acting as the structure-directing agents are occluded in the channels, and fluorine anions not only take part in the formation of $AlPO_4$-11 frameworks but also play the role of balancing the $[emim]^+$ cations.

ASSOCIATED CONTENT

Supporting Information

^{27}Al 3Q MAS NMR and $^1H \rightarrow {}^{31}P$ CP/MAS NMR spectra of solid samples. This material is available free of charge via the Internet at http://pubs.acs.org.

AUTHOR INFORMATION

Corresponding Author

*E-mail: wpzhang@dlut.edu.cn (W.Z.); xhbao@dicp.ac.cn (X.B.).

Notes

The authors declare no competing financial interest.

ACKNOWLEDGMENTS

We acknowledge the support of the National Natural Science Foundation of China (nos. 20873140, 21173029, 21103179), the Program for Liaoning Excellent Talents in University, and the Fundamental Research Funds for the Central Universities in China.

REFERENCES

(1) (a) Corma, A. *Chem. Rev.* **1995**, *95*, 559−614. (b) Davis, M. E. *Nature* **2002**, *417*, 813−821.

(2) (a) Aerts, A.; Kirschhock, C. E. A.; Martens, J. A. *Chem. Soc. Rev.* **2010**, *39*, 4626−4642. (b) Beale, A. M.; O'Brien, M. G.; Kasunic, M.; Golobic, A.; Sanchez-Sanchez, M.; Lobo, A. J. W.; Lewis, D. W.; Wragg, D. S.; Nikitenko, S.; Bras, W.; Weckhuysen, B. M. *J. Phys. Chem. C* **2011**, *115*, 6331−6340.

(3) Fan, F.; Feng, Z.; Li, C. *Chem. Soc. Rev.* **2010**, *39*, 4794−4801.

(4) Epping, J. D.; Chmelka, B. F. *Curr. Opin. Colloid Interface Sci.* **2006**, *11*, 81−117.

(5) (a) Martineau, C.; Bouchevreau, B.; Tian, Z.; Lohmeier, S.; Behrens, P.; Taulelle, F. *Chem. Mater.* **2011**, *23*, 4799−4809. (b) Huang, Y.; Richer, R.; Kirby, C. W. *J. Phys. Chem. B* **2003**, *107*, 1326−1337. (c) Sears, D. N.; Demko, B. A.; Ooms, K. J.; Wasylishen, R. E.; Huang, Y. N. *Chem. Mater.* **2005**, *17*, 5481−5488. (d) Xu, J.; Chen, L.; Zeng, D. L.; Yang, J.; Zhang, M. J.; Ye, C. H.; Deng, F. *J. Phys. Chem. B* **2007**, *111*, 7105−7113. (e) Xu, R.; Zhang, W.; Guan, J.; Xu, Y.; Wang, L.; Ma, H.; Tian, Z.; Han, X.; Lin, L.; Bao, X. *Chem.-Eur. J.* **2009**, *15*, 5348−5354. (f) Xu, R.; Shi, X.; Zhang, W.; Xu, Y.; Tian, Z.; Lu, X.; Han, X.; Bao, X. *Phys. Chem. Chem. Phys.* **2010**, *12*, 2443−2449. (g) Zhao, Z.; Zhang, W.; Xu, R.; Han, X.; Bao, X. *Dalton Trans.* **2012**, *41*, 990−994.

(6) Parnham, E. R.; Morris, R. E. *Acc. Chem. Res.* **2007**, *40*, 1005−1013.

(7) (a) Cooper, E. R.; Andrews, C. D.; Wheatley, P. S.; Webb, P. B.; Wormald, P.; Morris, R. E. *Nature* **2004**, *430*, 1012. (b) Parnham, E. R.; Morris, R. E. *J. Am. Chem. Soc.* **2006**, *128*, 2204. (c) Wheatley, P. S.; Allan, P. K.; Teat, S. J.; Ashbrook, S. E.; Morris, R. E. *Chem. Sci.* **2010**, *4*, 483−487. (d) Liu, L.; Li, Y.; Wei, H. B.; Dong, M.; Wang, J. G.; Slawin, A. M. Z.; Li, J. P.; Dong, J. X.; Morris, R. E. *Angew. Chem., Int. Ed.* **2009**, *48*, 2206−2209. (e) Wang, L.; Xu, Y.; Wei, Y.; Duan, J.; Chen, A.; Wang, B.; Ma, H.; Tian, Z.; Lin, L. *J. Am. Chem. Soc.* **2006**, *128*, 7432. (f) Xu, R.; Zhang, W.; Han, X.; Bao, X. *Chin. J. Catal.* **2010**, *31*, 776−780. (g) Li, K. D.; Tian, Z. J.; Li, X. L.; Xu, R. S.; Xu, Y. P.; Wang, L.; Ma, H. J.; Wang, B. C.; Lin, L. W. *Angew. Chem., Int. Ed.* **2012**, *51*, 4397−4400.

(8) (a) Amoureux, J. P.; Fernandez, C.; Steuernagel, S. *J. Magn. Reson. A* **1996**, *123*, 116. (b) Li, X. J.; Zhang, W. P.; Liu, S. L.; Xu, L. Y.; Han, X. W.; Bao, X. H. *J. Phys. Chem. C* **2008**, *112*, 5955−5960.

(9) Fyfe, C. A.; Mueller, K. T.; Grondey, H.; Wongmoon, K. C. *J. Phys. Chem.* **1993**, *97*, 13484−13495.

(10) Sayari, A.; Moudrakovski, I.; Reddy, J. S.; Ratcliffe, C. I.; Ripmeester, J. A.; Preston, K. F. *Chem. Mater.* **1996**, *8*, 2080−2088.

(11) Huang, Y. N.; Demko, B. A.; Kirby, C. W. *Chem. Mater.* **2003**, *15*, 2437−2444.

(12) Gougeon, R. D.; Brouwer, E. B.; Bodart, P. R.; Delmotte, L.; Marichal, C.; Chezeau, J. M.; Harris, R. K. *J. Phys. Chem. B* **2001**, *105*, 12249−12256.

(13) Mortlock, R. F.; Bell, A. T.; Radke, C. J. *J. Phys. Chem.* **1993**, *97*, 775−782.

(14) Burkett, S. L.; Davis, M. E. *J. Phys. Chem.* **1994**, *98*, 4647−4653.

(15) Villaescusa, L. A.; Wheatley, P. S.; Philip Lightfoot, I. B.; Morris, R. E. *J. Am. Chem. Soc.* **2001**, *123*, 8797−8805.

(16) Kirschhock, C. E. A.; Ravishankar, R.; Verspeurt, F.; Grobet, P. J.; Jacobs, P. A.; Martens, J. A. *J. Phys. Chem. B* **1999**, *103*, 4965−4971.

(17) Fyfe, C. A.; Darton, R. J.; Schneider, C.; Scheffler, F. *J. Phys. Chem. C* **2008**, *112*, 80−88.